Molecular architecture of the uncleaved HIV-1 envelope glycoprotein trimer

Youdong Mao[a,b,1], Liping Wang[a,b], Christopher Gu[a,b], Alon Herschhorn[a,b], Anik Désormeaux[c], Andrés Finzi[c], Shi-Hua Xiang[d], and Joseph G. Sodroski[a,b,e,f,1]

[a]Department of Cancer Immunology and AIDS, Dana-Farber Cancer Institute, Boston, MA 02215; [b]Department of Microbiology and Immunobiology, Harvard Medical School, Boston, MA 02115; [c]Centre de Recherche du Centre Hospitalier de l'Université de Montréal, Department of Microbiology and Immunology, Université de Montréal, Montréal, QC, Canada H3A 2B4; [d]Nebraska Center for Virology, School of Veterinary Medicine and Biomedical Sciences, University of Nebraska-Lincoln, Lincoln, NE 68583; [e]Ragon Institute of Massachusetts General Hospital, Massachusetts Institute of Technology, and Harvard, Cambridge, MA 02139; and [f]Department of Immunology and Infectious Diseases, Harvard School of Public Health, Boston, MA 02115

Edited* by Beatrice H. Hahn, University of Pennsylvania, Philadelphia, PA, and approved May 15, 2013 (received for review April 19, 2013)

The human immunodeficiency virus type 1 (HIV-1) envelope glycoprotein (Env) trimer, a membrane-fusing machine, mediates virus entry into host cells and is the sole virus-specific target for neutralizing antibodies. Binding the receptors, CD4 and CCR5/CXCR4, triggers Env conformational changes from the metastable unliganded state to the fusion-active state. We used cryo-electron microscopy to obtain a 6-Å structure of the membrane-bound, heavily glycosylated HIV-1 Env trimer in its uncleaved and unliganded state. The spatial organization of secondary structure elements reveals that the unliganded conformations of both glycoprotein (gp)120 and gp41 subunits differ from those induced by receptor binding. The gp120 trimer association domains, which contribute to interprotomer contacts in the unliganded Env trimer, undergo rearrangement upon CD4 binding. In the unliganded Env, intersubunit interactions maintain the gp41 ectodomain helical bundles in a "spring-loaded" conformation distinct from the extended helical coils of the fusion-active state. Quaternary structure regulates the virus-neutralizing potency of antibodies targeting the conserved CD4-binding site on gp120. The Env trimer architecture provides mechanistic insights into the metastability of the unliganded state, receptor-induced conformational changes, and quaternary structure-based strategies for immune evasion.

vaccine immunogen | retrovirus | spike | cryo-EM | membrane protein

Human immunodeficiency virus type 1 (HIV-1) is an enveloped retrovirus that causes AIDS (1, 2). To enter host cells, HIV-1 uses a metastable, trimeric envelope glycoprotein (Env) spike to engage cellular receptors and to fuse the viral and target cell membranes (3–5). During synthesis and folding in the endoplasmic reticulum of the virus-producing cell, the Env precursor [glycoprotein (gp)160] is heavily modified by *N*-linked glycosylation and assembles into trimers (6). In most HIV-1 strains, more than 27 potential *N*-linked glycosylation sites are present in each gp160 protomer. After further glycan processing in the Golgi apparatus, the gp160 Env trimer precursors are proteolytically cleaved and transported to the cell surface for incorporation into virions (7). Each protomer composing the trimeric Env spike thus consists of a gp120 exterior subunit and a gp41 transmembrane subunit. The sequential binding of gp120 to the target cell receptors, CD4 and chemokine receptor (either CCR5 or CXCR4), allows the metastable Env complex to transit into fusion-active conformations (3, 8–11). These conformational transitions expose the hydrophobic gp41 N-terminal fusion peptide, promoting its insertion into the target cell membrane, and further permit the formation of a highly stable gp41 six-helix bundle that mediates viral-cell membrane fusion (12–14). The Env spike is the only virus-specific component potentially accessible to neutralizing antibodies and thus has evolved a protective "glycan shield" and a high degree of interstrain variability.

High-resolution structures are available for monomeric HIV-1 gp120 core fragments in the CD4-bound conformation (15–18) and trimeric gp41 ectodomain fragments in the postfusion state (13, 18, 19). Only low-resolution structural information is available on the unliganded HIV-1 Env trimer (20–23), despite its importance as the major target for vaccine-induced neutralizing antibodies. Heavy glycosylation, unusual metastability, and structural plasticity have frustrated efforts to obtain a high-resolution structure. Recently we developed methods to purify a membrane-bound HIV-1 Env trimer [Env(-)ΔCT] and used single-particle cryo-electron microscopy (cryo-EM) to obtain an 11-Å structure of the unliganded trimer (24). The purified and detergent-protected Env(-)ΔCT trimer, which is derived from the primary, neutralization-resistant HIV-1_{JR-FL} isolate, has two residue changes (R508S and R511S) to eliminate gp120–gp41 proteolytic cleavage and has the cytoplasmic tail (CT) truncated (24). The 11-Å cryo-EM structure of the Env(-)ΔCT trimer is consistent with electron tomographic maps of the functional Env spike on virions (20), suggesting that the Env(-)ΔCT structure may capture the unliganded conformation of the native Env trimer. The organization of the gp120 and gp41 subunits in the Env trimer, the spatial relationship of Env domains, and the existence of a remarkable central void were evident in the 11-Å structure (24). However, at this resolution it was impossible to distinguish secondary structure elements or to appreciate their 3D organization in the Env trimer. Here we report a 6-Å cryo-EM structure of the fully glycosylated HIV-1_{JR-FL} Env(-)ΔCT trimer complex in an unliganded state (Movies S1 and S2). Visualization of the spatial organization of the secondary structural elements in the 6-Å density map reveals the unique architecture of the Env trimer and facilitates a mechanistic understanding of HIV-1 entry and immune evasion.

Results

Structure Determination. We used the 11-Å structure of the HIV-1_{JR-FL} Env(-)ΔCT trimer (24) as an initial reference to refine the cryo-EM structure from 670,000 single-particle images of detergent-solubilized purified trimers by a projection matching algorithm. The resolution of the refined density map was estimated to be ~6 Å by Fourier shell correlation at 0.5 cutoff (Fig. S1). Consistent with this estimate, heretofore unseen features associated with secondary structure elements were apparent in the density map. The α-helices and β-sheets could be identified and were mostly separated from each other (Figs. S2–S5). We were able to position the majority of

Author contributions: Y.M. and J.G.S. designed research; Y.M., L.W., C.G., A.H., A.D., A.F., and S.-H.X. performed research; Y.M. and J.G.S. analyzed data; and Y.M. and J.G.S. wrote the paper.

The authors declare no conflict of interest.

*This Direct Submission article had a prearranged editor.

Freely available online through the PNAS open access option.

Data deposition: The cryo-EM map of the uncleaved HIV-1 envelope trimer was deposited into the EMDataBank, www.emdatabank.org (accession no. EMD-5447).

[1]To whom correspondence may be addressed: E-mail: youdong_mao@dfci.harvard.edu or joseph_sodroski@dfci.harvard.edu.

This article contains supporting information online at www.pnas.org/lookup/suppl/doi:10.1073/pnas.1307382110/-/DCSupplemental.

secondary structure elements and, in conjunction with available structural information, to approximate the tertiary organization of Env (Fig. 1). However, as expected, the adjacent strands within the β-sheets were not separable at this resolution. Connecting loops often exhibited poor clarity or were not separable from nearby structures, preventing a complete backbone trace from being unambiguously derived at the current resolution. In addition to the appearance of features indicative of secondary structure elements, the rigid-body fitting of the X-ray crystal structure of the gp120 outer domain into the density supports the validity of the cryo-EM reconstruction (see below).

Overview of Env Molecular Architecture. The gp120 and gp41 subunits and their intersubunit interfaces were discernable and approximately defined by map segmentation (Fig. 1 *C* and *D*). The gp120 subunit demonstrates three domains: the outer domain, inner domain, and trimer association domain (TAD). The gp41 subunit is composed of the ectodomain and the membrane-interactive region, which includes a long membrane-spanning helix. The gp120 inner domain and the membrane-distal end of the gp41 ectodomain mediate the gp120–gp41 interactions within each protomer. The interprotomer interactions that potentially stabilize the unliganded Env trimer are limited to three regions: (*i*) the gp41 transmembrane region is involved in a trimeric interface within the viral membrane; (*ii*) the gp41 ectodomain forms dimeric contacts between adjacent protomers, creating a torus-like topology; and (*iii*) the gp120 TAD mediates interactions among the gp120 subunits at the membrane-distal end of the trimer. Remarkably, this arrangement of interprotomer contacts leaves a large empty space surrounding most of the trimer axis.

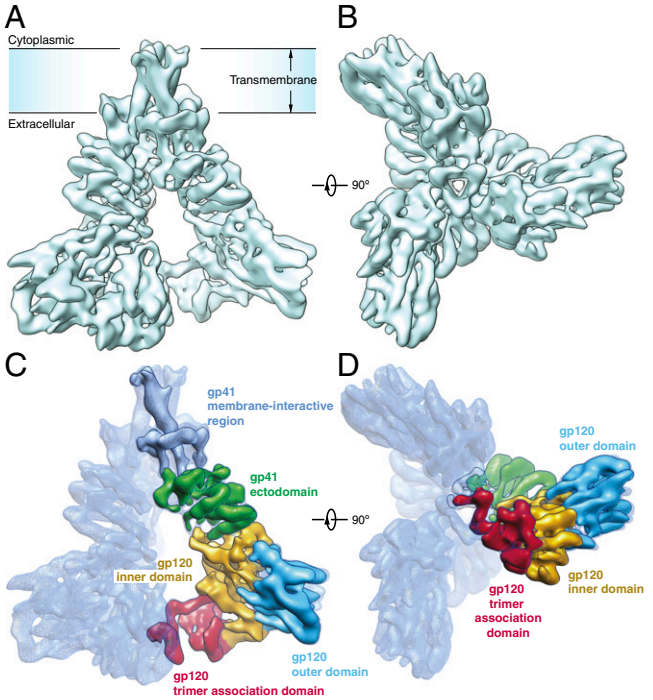

Fig. 1. Architecture of the HIV-1 Env trimer. (*A*) Cryo-EM map of the HIV-$1_{JR\text{-}FL}$ Env trimer in a surface representation, viewed from a perspective parallel to the viral membrane. (*B*) Cryo-EM map of the HIV-$1_{JR\text{-}FL}$ Env trimer, viewed from the perspective of the target cell. (*C* and *D*) Domain organization of the Env protomer, revealed by segmentation of the density map. The gp120 domains are colored as follows: outer domain, blue; inner domain, orange; and TAD, red. The gp41 domains are colored as follows: ectodomain, green; and transmembrane region, cyan.

Unliganded gp120 and CD4-Induced Conformational Changes. The CD4-bound gp120 core consists of an inner and outer domain, as well as a bridging sheet (16). The full-length unliganded gp120 subunit shown in our cryo-EM map exhibits a conformation different from that observed in the CD4-bound gp120 core (16). The improved resolution of the current map allows positioning of the secondary structure elements in gp120 and a detailed assessment of the conformational changes collectively associated with Env cleavage and CD4 binding (25–28).

Multiple crystal structures of the monomeric gp120 core indicate that the conformation of the outer domain is minimally affected by ligand binding (15, 16, 29–32). Consistent with this, the crystal structure of the outer domain from the CD4-bound gp120 core fit well into the cryo-EM density as a rigid body (Fig. 2 *A* and *B*, Fig. S3 *A* and *B*, and Table S1). Two gp120 elements, the β20/β21 strands and the V3 variable region, project from the same β-sheet in the outer domain (16). Density associated with these elements is evident in the cryo-EM map, and the size difference of these elements (~14 residues vs. 35 residues, respectively) allows their provisional assignment. In the unliganded Env trimer, the β20/β21 strands project toward and abut the gp120 inner domain, whereas the V3 region joins the gp120 TAD. Upon CD4 binding, β20/β21 becomes part of the bridging sheet, and the V3 region is redirected toward the target cell, where it engages the chemokine receptor (33).

In contrast to the outer domain, the crystal structure of the gp120 inner domain did not fit into the cryo-EM density as a rigid body. However, we approximated the secondary structure organization of the gp120 inner domain in the cryo-EM map by flexibly fitting the crystal structure of the gp120 inner domain in the CD4-bound conformation to our cryo-EM map (Fig. 2 *C*–*E*). Although the limited resolution precludes a complete backbone trace of the gp120 inner domain, most of the secondary structure elements in the CD4-bound gp120 inner domain seem to be retained in the cryo-EM structure of the unliganded Env trimer (Fig. 2 *C* and *D*, Fig. S3 *C* and *D*, and Table S1). However, comparison of the secondary structure organization of the gp120 inner domain between the unliganded precursor and CD4-bound states suggests marked differences in the tertiary arrangements of these secondary structure elements (Fig. 2 *E* and *F* and Fig. S4). Relative to the gp120 outer domain, the β-sandwich in the gp120 inner domain is rotated by ~60° in the unliganded precursor state compared with the CD4-bound state (Fig. 2 *E* and *F*). The α0, α1, and α5 helices are rotated ~110°, 40°, and 60° relative to their orientations in the CD4-bound conformation, respectively (Fig. S4). These observations are consistent with previous studies suggesting that layered movement occurs within the gp120 inner domain upon CD4 binding (17, 25, 28).

A recent study suggested that the bridging sheet (β2/β3 and β20/β21), which was observed in the crystal structure of the monomeric gp120 core in the CD4-bound state (16), is not well formed in the unliganded full-length gp120 monomer in solution (34). Consistent with this suggestion, flexible fitting of the CD4-bound gp120 core structure to our unliganded Env precursor map failed to maintain the bridging sheet in its CD4-bound conformation (Fig. 2*E* and Fig. S3). Instead, the β2/β3 motif, from which the gp120 V1/V2 region emanates, must extend from the inner domain toward the trimer axis to accommodate the folding of the V1/V2 and V3 regions (see the following section) (Fig. S3 *E* and *F*). The map density associated with β20/β21 suggests that it projects from the outer domain toward the inner domain, oriented nearly orthogonally to β2/β3 (Fig. 2 *D* and *E*). Thus, both the bridging sheet and the inner domain represent dynamic elements of the gp120 subunit, undergoing significant changes in conformation in response to CD4 binding.

Architecture of gp120 Trimer Association. Previous studies have suggested that the gp120 V1, V2, and V3 regions (20, 23, 24) are located at the membrane-distal apex of the Env spike and

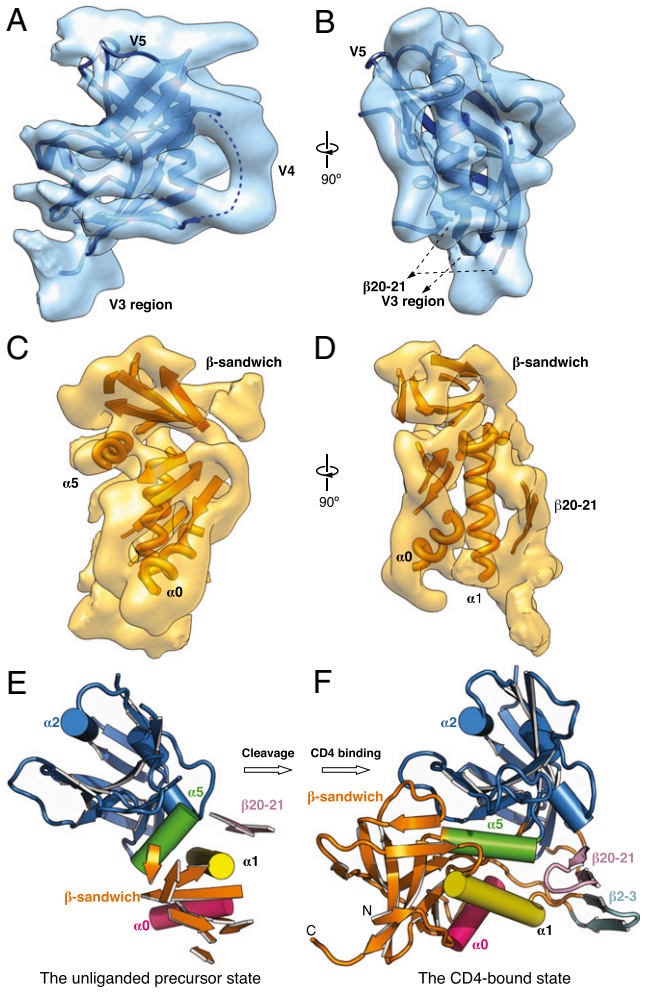

Fig. 2. The unliganded gp120 subunit and CD4-induced changes. (*A* and *B*) Crystal structure of the outer domain of the gp120 core (17) was fitted into the cryo-EM map of the unliganded Env trimer and is shown from two perspectives parallel to the viral membrane. The approximate location of the V4 variable region, which was not resolved in the crystal structure, is indicated by a broken line. (*C* and *D*) Secondary structure organization of the inner domain of gp120 was approximated in the cryo-EM map of the unliganded Env trimer, which is viewed from two perspectives parallel to the viral membrane. (*E* and *F*) For comparison of the unliganded precursor state (*E*) and the CD4-bound state (*F*) of the gp120 core, the gp120 outer domains (blue) are aligned in the same orientation. The gp120 core in the unliganded precursor state is derived as described in *A*–*D* above, and the CD4-bound gp120 core structure is from an X-ray crystal structure (Protein Data Bank ID: 3JWD).

contribute to the association of gp120 with the trimer (35, 36). The flexible fitting of the gp120 core structure in our cryo-EM map demarcates the boundary of the gp120 TAD that comprises the V1, V2, and V3 regions (24). The TAD in each protomer exhibits a β-α-β architecture and extends transversely from the gp120 inner domain to the trimer axis (Fig. 3*A*). Occupying this span is an α-helix ∼2 nm long stacked against a tilted β-sheet-like motif; the V1/V2 stem (β2/β3) and the V3 region enter this β-sheet from the inner and outer gp120 domains, respectively (Fig. 3 *B* and *C*). This transverse α-β structure supports a β-sheet-like leaf, which joins its counterparts from the other protomers to form a barrel-like structure at the trimer center (Fig. 3 *B* and *C*). The TAD architecture and, by inference, gp120 association with the trimer, apparently depend upon multiple interactions among secondary structure elements formed by the V1, V2, and V3 regions.

The broadly neutralizing antibodies Protocol G (PG)9 and PG16 recognize glycan-dependent TAD epitopes and exhibit a strong quaternary-structure preference for Env trimers (37), consistent with the complex architecture of this region. When removed from the context of the Env trimer, significant portions of the V1, V2, and V3 regions become disordered (33), and recognition by the PG9 and PG16 antibodies is markedly diminished (37). By expressing the V1/V2 region fused with a heterologous scaffold protein and using an elegant strategy to select complexes with PG9, a crystal structure was obtained (38). We can fit the two V1/V2 β-strands in immediate contact with the PG9 antibody into the Env trimer map, although the complete V1/V2 region from this crystal structure cannot be accommodated. We note that a considerable portion of the V1/V2 region remains disordered and is not resolved in the crystal structure. Interactions with other elements of the TAD, the inner domain, or other protomers in the trimer may promote folding of these V1/V2 elements into distinct structures.

Transmembrane Region of the gp41 Subunit. The gp41 transmembrane region anchors the Env spike to the viral membrane and acts as a pivot point for interactions among the three protomeric arms. The membrane-spanning segment of each protomer is consistent with an α-helix. The three α-helices form a left-handed coiled coil, with a crossing angle of ∼35° (Fig. 4 *A* and *B* and Fig. S5 *A* and *B*). The chirality of the transmembrane helical bundle is compatible with that of the gp41 ectodomain core structure in the postfusion state (12, 13, 18).

The transmembrane α-helical coiled coil extends beyond the boundary of the viral membrane into the membrane-proximal external region (Fig. 4 *A* and *B* and Fig. S5*B*). Near the surface of the viral membrane, transverse segments of structure, likely composed of short α-helices and loops emanating from and returning to the gp41 ectodomain, wedge into the transmembrane helical bundle close to the trimer axis. The resulting structure not only stabilizes the transmembrane helical bundle but also creates a sufficiently wide pitch and appropriate crossing angle between the three interacting α-helices so that the gp41 ectodomain can be built upon the transmembrane helices and achieve its torus-like topology (24).

Ectodomain of the gp41 Subunit. With an overall globular shape, the gp41 ectodomain from each protomer comprises potentially seven major α-helical elements (Fig. 4 and Fig. S5 *C* and *D*). One additional α-helix packed into this helical bundle could be assigned to either gp41 or the gp120 N/C termini. The interprotomer interactions between the gp41 ectodomains incorporate the

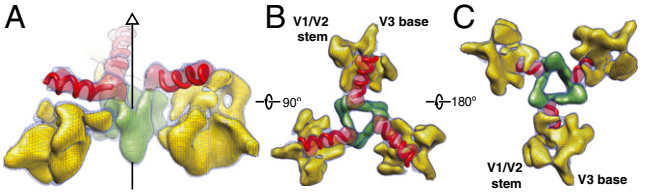

Fig. 3. Architecture of the gp120 TAD. (*A*) Secondary structure elements in the gp120 TAD, viewed from a perspective perpendicular to the Env trimer axis. The TAD comprises an α-helix (red), a minibarrel structure (green), and a β-sheet-like element (yellow). (*B*) Three helical elements (red) pointing toward the central minibarrel structure (green), viewed from the center of mass of the trimer. (*C*) The TAD, viewed from the perspective of the target cell. The points at which the V1/V2 stem and V3 loop enter the TAD from the gp120 inner domain and outer domain, respectively, are indicated. The map segmentations of the gp120 TAD are shown as blue meshwork for a lower level of contour and as solid surfaces for slightly higher levels of contour. The potential α-helical elements shown as worm tubes are schematically illustrated and are not intended to represent definitive backbone traces.

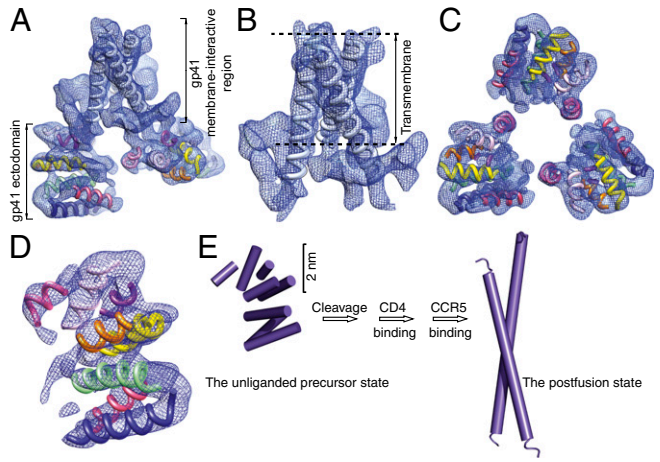

Fig. 4. gp41 subunit in the Env trimer. (*A*) Cryo-EM map of the three gp41 subunits in the Env trimer, viewed from an angle of ~30° with respect to the viral membrane. (*B*) gp41 membrane-interactive region viewed from a perspective parallel to the viral membrane. (*C*) gp41 ectodomain, viewed from the perspective of the virus. The torus-like topology of the three gp41 subunits in the Env trimer is evident from this perspective. (*D*) gp41 ectodomain, viewed from a perspective parallel to the viral membrane. (*E*) Comparison of the gp41 ectodomain in the unliganded precursor state and the postfusion state with respect to the tertiary organization of helices. The perspective is identical to that shown in *D*, with a reduction in scale. For simplicity, only one of the three gp41 glycoprotein subunits in the Env trimer is depicted.

membrane-proximal α-helical elements into a trilobed torus (Fig. 4 *A* and *C* and Fig. S5 *A* and *C*). From this torus-like substructure, the membrane-distal α-helical gp41 elements spread away from the trimer axis and compose the interface with gp120 (Figs. 1*C* and 4*A* and Fig. S5*A*).

The organization of secondary structure elements in the gp41 ectodomain in this unliganded and uncleaved state of Env differs dramatically from that of the six-helix bundle structure seen in the postfusion state (12–14, 18, 19) (Fig. 4 *D* and *E* and Fig. S5*D*). In the six-helix bundle, three heptad repeat 1 (HR1) regions (residues ~546–581) assemble into a trimeric coiled coil and three HR2 regions (residues ~628–661) form long α-helices that pack in an antiparallel fashion into the hydrophobic grooves of the coiled coil. In the unliganded state of Env, the long HR1 and HR2 α-helices in the six-helix bundle seem to be broken into short helices (Fig. 4 and Fig. S5), consistent with previous suggestions that the trimeric coiled coil is not formed before CD4 engagement (39, 40). Although the assignment of primary sequence to the gp41 ectodomain α-helices will require higher-resolution structures, the available evidence supports a model in which (*i*) α-helical elements from the HR1 region locate at the membrane-distal end of the ectodomain and interact with the gp120 subunit; and (*ii*) α-helical elements from the HR2 region locate around the membrane-proximal end of the ectodomain, contribute to the gp41 trimeric interactions, and constitute the torus-shaped structure. Consistent with this model, mutagenesis experiments implicate the HR1 region in the noncovalent association with gp120 (41) and the HR2 region in trimerization of the Env ectodomain (42).

Env Glycosylation. *N*-linked carbohydrates constitute approximately 47% of the molecular weight of the fully glycosylated HIV-1 Env complex. *N*-linked glycans are largely disordered in free solution. Although it is expected that the cryo-EM reconstruction would average out most of the peptide-distal glycan density, part of the peptide-proximal glycans must conform to the protein structure and retain a certain degree of structural order. Rigid-body fitting of the crystal structure of the gp120 outer domain into the cryo-EM map revealed a number of outward-protruding densities on the surface of the gp120 outer domain (Fig. 5 *A* and *B* and Fig. S6). These extra densities can be attributed to the peptide-proximal glycan residues common to the trimannosyl cores of both high-mannose and complex types of *N*-linked oligosaccharide (Fig. 5*C*). Notably, the locations of these protuberances were found to strictly correspond to the potential *N*-linked glycosylation sites (PNGS) in the crystal structure of the gp120 outer domain (Fig. 5 and Fig. S6). The agreement of the spatial positions of the identified glycan density in the cryo-EM map with those of the PNGS in the crystal structure of the gp120 outer domain provides an independent validation for the cryo-EM reconstruction.

Role of Quaternary Structure in Antibody Evasion. The CD4-binding site (CD4BS) antibodies are elicited in HIV-1–infected individuals, are directed against the conserved gp120 surface that engages CD4, and exhibit a range of potencies in HIV-1 neutralization (43, 44). The available crystal structures of several CD4BS antibodies complexed with the HIV-1 gp120 core provide information about their preferred binding mode (29–31, 45). As noted above, the overall conformation of the gp120 outer domain in the unliganded HIV-1 Env trimer does not significantly differ from that in the crystal structures of gp120 cores complexed with CD4BS antibodies. All CD4BS antibodies include gp120 outer domain elements in their epitopes. The gp120 outer domains of the crystal structures of the antibody-bound gp120 core were superposed on the outer domain of the uncleaved Env trimer. Assuming the uncleaved Env trimer structure approximates the equilibrium conformation of the mature unliganded Env spike on virions, we could thus assess the angle-of-approach and steric hindrance experienced by the CD4BS antibodies during their initial engagement with the Env trimer. The results reveal remarkable differences among CD4BS antibodies (Fig. 6). The potently neutralizing antibodies VRC01, VRC03, VRC-PG04, and NIH 45-46 experience nearly no quaternary steric hindrance from the neighboring Env subunit (Fig. 6 *A* and *B* and Fig. S7). By contrast, the neighboring Env subunit creates substantial quaternary steric hindrance for the b12, b13, and F105 antibodies, suggesting that an induced conformational change in the Env trimer is necessary for these less potently neutralizing antibodies to achieve optimal binding. Fig. 6*F* shows that the predicted degree of quaternary steric hindrance encountered by the CD4BS antibodies as they engage the unliganded Env trimer, using b12 binding as a normalization metric, is inversely related to HIV-1 neutralization potency. This correlation supports the relevance of the Env(-)ΔCT

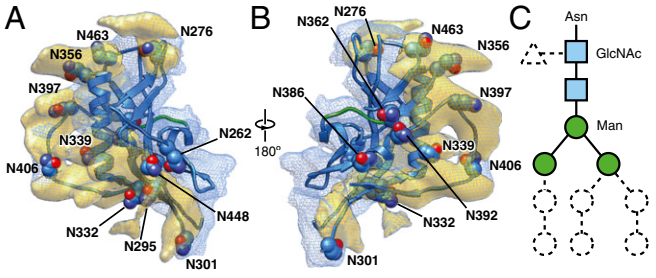

Fig. 5. Env glycosylation. (*A* and *B*) Glycan-associated densities on the gp120 surface, viewed from two perspectives parallel to the viral membrane. The gp120 outer domain ribbon is colored blue and the asparagine residues associated with potential *N*-linked glycosylation sites are shown in Corey-Pauling-Koltun (CPK) representation and labeled. The blue meshwork shows the overall map segment associated with the gp120 outer domain. The yellow densities highlight the potential glycan-associated map segments in a surface representation. (*C*) Schematic showing the five glycan core residues associated with *N*-linked glycosylation. The trimannosyl core, which is common to high-mannose, complex, and hybrid oligosaccharides, is colored.

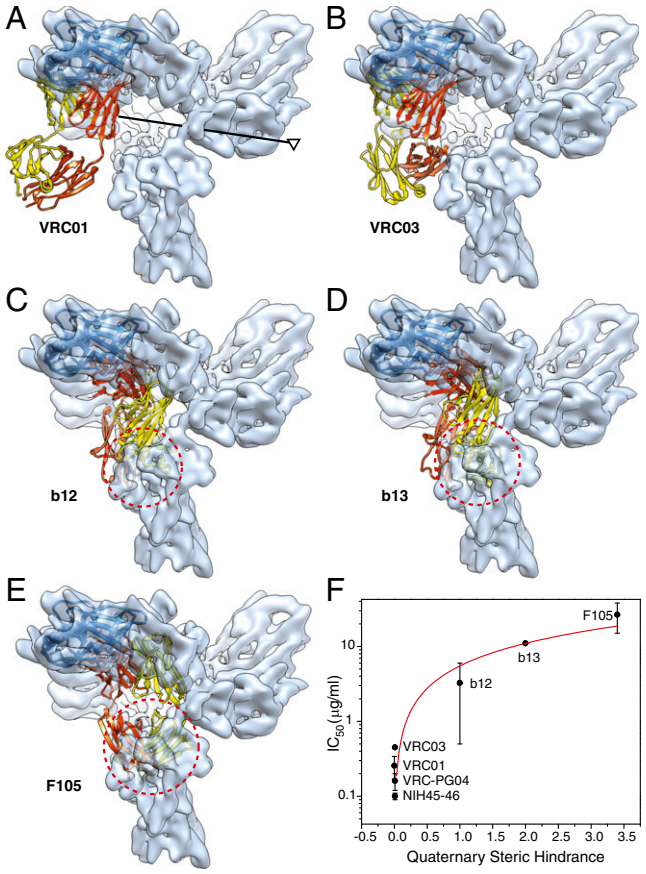

Fig. 6. Effect of quaternary structure on virus neutralization by CD4BS antibodies. (*A*–*E*) Crystal structures of the gp120 core in complex with the CD4BS antibodies, VRC01 (*A*), VRC03 (*B*), b12 (*C*), b13 (*D*), and F105 (*E*) were superposed on the unliganded Env precursor map, with the Env trimer axis shown in *A*. The conformationally rigid gp120 outer domain was fitted to the Env trimer density map, and the outer domains in the crystal structures were aligned with the fitted outer domain (represented as a blue ribbon). The heavy and light chains of the CD4BS antibodies are colored red and yellow, respectively. The dashed red circle in *C*–*E* marks the approximate diameter of the space in the neighboring gp120 subunit that is overlapped by the antibodies, highlighting the quaternary steric hindrance that the antibodies experience when approaching their binding site on the gp120 outer domain. (*F*) Using the volume of the quaternary clash in the case of b12 as a normalization metric, the degree of quaternary steric hindrance encountered by each antibody as it accesses the Env trimer was quantified and was plotted against the geometric mean IC_{50} of the neutralization of multiple HIV-1 strains by the antibody (29–31, 43–45). The Protein Data Bank IDs of the antibodies in complex with gp120 core structures are 3NGB (*A*), 3SE8 (*B*), 2NY7 (*C*), 3IDX (*D*), and 3HI1 (*E*). The red line shows a linear regression of the relationship (rS: 0.9985, slope: 5.5, SE: 0.082).

trimer structure to that of the functional virion Env spike. Our results provide a structural explanation for experimental observations suggesting that the ability to bind the Env trimer in its unliganded state represents a major factor in determining the neutralization potency of CD4BS antibodies (29, 46–48).

Discussion

Here we present a 6-Å structure of the unliganded HIV-$1_{JR\text{-}FL}$ Env(-)ΔCT glycoprotein, a membrane-anchored, uncleaved Env trimer with a truncated CT. We have previously shown that these detergent-solubilized purified Env trimers exhibit affinities for multiple conformation-dependent neutralizing antibodies comparable to those of the uncleaved Env trimer expressed on the cell surface (24). Binding assays using an expanded panel of both neutralizing and nonneutralizing antibodies targeting either gp120 or gp41 further corroborated the antigenic relatedness of the purified and cell-surface Env(-)ΔCT glycoproteins (Fig. S8). Thus, the Env(-)ΔCT trimer preserves its conformation upon detergent solubilization and exhibits the antigenic profile expected of the uncleaved HIV-1 Env precursor (46, 48). Proteolytic cleavage has been reported to decrease the conformational entropy of the Env trimer and to impede selectively the binding of nonneutralizing or weakly neutralizing antibodies (46, 48). The compatibility of low-resolution 3D models of the Env(-)ΔCT trimer and the full-length, proteolytically mature Env trimer on the HIV-1 virion suggests that the global conformation of the Env trimer is not substantially altered by proteolytic cleavage or the presence of the CT (20, 24). However, higher-resolution information will be required to characterize the subtle changes in Env conformational entropy and/or structure associated with proteolytic maturation or the influence of the CT (Fig. S9).

Enveloped viruses use conformational changes in their envelope proteins to mediate the fusion of viral and target cell membranes. Environmental triggers such as a pH decrease or receptor binding drive the envelope proteins to energetically favorable, fusion-ready conformations. Influenza virus uses low pH, which globally alters the conformation of the HA protein, as a trigger. A spring-loaded mechanism has been suggested to explain the HA conformational change that mediates virus entry (49, 50). The long α-helix in the fusion-ready HA_2 protein is broken into several shorter pieces in the prefusion state, resembling a "loaded spring." When triggered by a pH decrease, the HA_2 short helices and linking loops refold into a longer helix of lower free energy. This allosteric change delivers the fusion peptide at the HA_2 N terminus to the target membrane and promotes virus entry.

Instead of a decrease in pH, HIV-1 uses sequential binding to the CD4 and CCR5/CXCR4 receptors as triggers for entry-priming conformational changes in Env (5). The unliganded Env trimer is prestressed, storing the free energy needed for membrane fusion in its unique architecture. Spring loading seems to be used twice in the unliganded gp41 subunit: the HR1 and HR2 helices of the postfusion six-helix bundle are each broken into smaller helices and other structural elements in the membrane-distal gp120–gp41 interaction interface and in the membrane-proximal torus, respectively. This dual spring-loaded mechanism likely reflects the unique requirements of stepwise activation by dual receptor engagement, so that binding to each receptor frees only one "spring" at a time. Consistent with this model, experimental observations suggest that CD4 binding induces the formation and exposure of the HR1 coiled coil, but subsequent events such as CCR5/CXCR4 binding are required for formation of HR2 and the six-helix bundle (8, 39, 40).

Achieving a prestressed structure that implements a dual spring-loaded mechanism imposes significant challenges to glycoprotein folding; indeed, HIV-1 Env synthesis and assembly is relatively slow and inefficient (6, 7). Once synthesized, functional Env spikes must avoid being prematurely triggered. Synthesis and maintenance of a competent, spring-loaded Env trimer requires multiple interactions between and within the subunits. The elegant torus-like architecture of gp41 takes advantage of the high stability and pivot potential of the transmembrane three-helix bundle. Truncations of the gp41 transmembrane region to produce "soluble gp140" trimers (51, 52) typically disrupt the native Env structure, as indicated by loss of the PG9 and PG16 epitopes (37). Building upon the gp41 torus-like architecture, noncovalent interactions with the gp120 inner domain and N/C termini likely maintain the spring-loaded conformation of the membrane-distal gp41 ectodomain. Interactions between the TAD and the gp120 inner domain potentially explain the ability of the V1/V2 and V3 regions to prevent gp120 from assuming the energetically favored CD4-bound state (15). Conversely, CD4 binding necessitates TAD restructuring, thus reducing gp120 trimerization and allowing an open conformation of the trimer (20). The "spring-loaded"

architecture of the HIV-1 Env is well adapted to respond to the relatively subtle perturbation of initial receptor engagement with dramatic, programmed conformational changes. Sensitive adjustment of local features allows HIV-1 variants to adapt to differing levels of receptors and to escape antibody neutralization. Thus, the unique architecture of the Env trimer offers multiple fitness advantages to a persistent virus like HIV-1.

Materials and Methods

Expression and purification of the HIV-1_{JR-FL} Env(-)ΔCT glycoprotein have been previously described (24). Cryo-EM data were collected with a FEI Tecnai F20. Details of experimental procedure, data collection, data processing, and cryo-EM reconstruction are described in *SI Materials and Methods*.

ACKNOWLEDGMENTS. We thank P. Kwong, J. Robinson, P. Poignard, S. Zolla-Pazner, H. Katinger, M. Posner, and L. Cavacini for kindly providing antibodies; D. R. Burton for helpful discussion and encouragement; A. Leschziner for help in cryo-specimen preparation; D. Bell and E. Hodges for coordination in data collection; J. Faltskog, S. Doktor, and B. Battle for laboratory coordination; J. Jackson and B. Richter for assistance in building and maintaining the high-performance computing system; and Y. McLaughlin and E. Carpelan for assistance in manuscript preparation. The experiments and data processing were performed in part at the Center for Nanoscale Systems at Harvard University, a member of National Nanotechnology Infrastructure Network, which is supported by the National Science Foundation (NSF) under NSF Award ECS-0335765. This work was funded by National Institutes of Health Grants AI93256, AI67854, and AI24755, by an Innovation Award and a Fellowship Award from the Ragon Institute of Massachusetts General Hospital, Massachusetts Institute of Technology, and Harvard, by the International AIDS Vaccine Initiative, and by gifts from Mr. and Mrs. Daniel J. Sullivan, Jr. and the late William F. McCarty-Cooper. A.H. is the recipient of a Mathilde Krim Fellowship in Basic Science from the American Foundation for AIDS Research. A.F. is the recipient of a Canada Foundation for Innovation Program Leader (#29866), a Canadian Institutes of Health Research operating (#257792) and an Fonds de Recherche en Santé du Québec Chercheur Boursier Junior 1 fellowship (#24639).

1. Barré-Sinoussi F, et al. (1983) Isolation of a T-lymphotropic retrovirus from a patient at risk for acquired immune deficiency syndrome (AIDS). *Science* 220(4599):868–871.
2. Gallo RC, et al. (1984) Frequent detection and isolation of cytopathic retroviruses (HTLV-III) from patients with AIDS and at risk for AIDS. *Science* 224(4648):500–503.
3. Allan JS, et al. (1985) Major glycoprotein antigens that induce antibodies in AIDS patients are encoded by HTLV-III. *Science* 228(4703):1091–1094.
4. Robey WG, et al. (1985) Characterization of envelope and core structural gene products of HTLV-III with sera from AIDS patients. *Science* 228(4699):593–595.
5. Wyatt R, Sodroski J (1998) The HIV-1 envelope glycoproteins: Fusogens, antigens, and immunogens. *Science* 280(5371):1884–1888.
6. Fennie C, Lasky LA (1989) Model for intracellular folding of the human immunodeficiency virus type 1 gp120. *J Virol* 63(2):639–646.
7. Moulard M, Decroly E (2000) Maturation of HIV envelope glycoprotein precursors by cellular endoproteases. *Biochim Biophys Acta* 1469(3):121–132.
8. Furuta RA, Wild CT, Weng Y, Weiss CD (1998) Capture of an early fusion-active conformation of HIV-1 gp41. *Nat Struct Biol* 5(4):276–279.
9. Koshiba T, Chan DC (2003) The prefusogenic intermediate of HIV-1 gp41 contains exposed C-peptide regions. *J Biol Chem* 278(9):7573–7579.
10. He Y, et al. (2003) Peptides trap the human immunodeficiency virus type 1 envelope glycoprotein fusion intermediate at two sites. *J Virol* 77(3):1666–1671.
11. Si Z, et al. (2004) Small-molecule inhibitors of HIV-1 entry block receptor-induced conformational changes in the viral envelope glycoproteins. *Proc Natl Acad Sci USA* 101(14):5036–5041.
12. Chan DC, Fass D, Berger JM, Kim PS (1997) Core structure of gp41 from the HIV envelope glycoprotein. *Cell* 89(2):263–273.
13. Weissenhorn W, Dessen A, Harrison SC, Skehel JJ, Wiley DC (1997) Atomic structure of the ectodomain from HIV-1 gp41. *Nature* 387(6631):426–430.
14. Melikyan GB, et al. (2000) Evidence that the transition of HIV-1 gp41 into a six-helix bundle, not the bundle configuration, induces membrane fusion. *J Cell Biol* 151(2):413–423.
15. Kwon YD, et al. (2012) Unliganded HIV-1 gp120 core structures assume the CD4-bound conformation with regulation by quaternary interactions and variable loops. *Proc Natl Acad Sci USA* 109(15):5663–5668.
16. Kwong PD, et al. (1998) Structure of an HIV gp120 envelope glycoprotein in complex with the CD4 receptor and a neutralizing human antibody. *Nature* 393(6686):648–659.
17. Pancera M, et al. (2010) Structure of HIV-1 gp120 with gp41-interactive region reveals layered envelope architecture and basis of conformational mobility. *Proc Natl Acad Sci USA* 107(3):1166–1171.
18. Buzon V, et al. (2010) Crystal structure of HIV-1 gp41 including both fusion peptide and membrane proximal external regions. *PLoS Pathog* 6(5):e1000880.
19. Tan K, Liu J, Wang J, Shen S, Lu M (1997) Atomic structure of a thermostable subdomain of HIV-1 gp41. *Proc Natl Acad Sci USA* 94(23):12303–12308.
20. Liu J, Bartesaghi A, Borgnia MJ, Sapiro G, Subramaniam S (2008) Molecular architecture of native HIV-1 gp120 trimers. *Nature* 455(7209):109–113.
21. White TA, et al. (2010) Molecular architectures of trimeric SIV and HIV-1 envelope glycoproteins on intact viruses: Strain-dependent variation in quaternary structure. *PLoS Pathog* 6(12):e1001249.
22. Wu SR, et al. (2010) Single-particle cryoelectron microscopy analysis reveals the HIV-1 spike as a tripod structure. *Proc Natl Acad Sci USA* 107(44):18844–18849.
23. Hu G, Liu J, Taylor KA, Roux KH (2011) Structural comparison of HIV-1 envelope spikes with and without the V1/V2 loop. *J Virol* 85(6):2741–2750.
24. Mao Y, et al. (2012) Subunit organization of the membrane-bound HIV-1 envelope glycoprotein trimer. *Nat Struct Mol Biol* 19(9):893–899.
25. Finzi A, et al. (2010) Topological layers in the HIV-1 gp120 inner domain regulate gp41 interaction and CD4-triggered conformational transitions. *Mol Cell* 37(5):656–667.
26. Myszka DG, et al. (2000) Energetics of the HIV gp120-CD4 binding reaction. *Proc Natl Acad Sci USA* 97(16):9026–9031.
27. Sattentau QJ, Moore JP (1991) Conformational changes induced in the human immunodeficiency virus envelope glycoprotein by soluble CD4 binding. *J Exp Med* 174(2):407–415.
28. Désormeaux A, et al. (2013) The highly conserved layer-3 component of the HIV-1 gp120 inner domain is critical for CD4-required conformational transitions. *J Virol* 87(5):2549–2562.
29. Chen L, et al. (2009) Structural basis of immune evasion at the site of CD4 attachment on HIV-1 gp120. *Science* 326(5956):1123–1127.
30. Zhou T, et al. (2007) Structural definition of a conserved neutralization epitope on HIV-1 gp120. *Nature* 445(7129):732–737.
31. Zhou T, et al. (2010) Structural basis for broad and potent neutralization of HIV-1 by antibody VRC01. *Science* 329(5993):811–817.
32. Chen B, et al. (2005) Structure of an unliganded simian immunodeficiency virus gp120 core. *Nature* 433(7028):834–841.
33. Huang CC, et al. (2005) Structure of a V3-containing HIV-1 gp120 core. *Science* 310(5750):1025–1028.
34. Guttman M, Kahn M, Garcia NK, Hu SL, Lee KK (2012) Solution structure, conformational dynamics, and CD4-induced activation in full-length, glycosylated, monomeric HIV gp120. *J Virol* 86(16):8750–8764.
35. Sullivan N, Thali M, Furman C, Ho DD, Sodroski J (1993) Effect of amino acid changes in the V1/V2 region of the human immunodeficiency virus type 1 gp120 glycoprotein on subunit association, syncytium formation, and recognition by a neutralizing antibody. *J Virol* 67(6):3674–3679.
36. Xiang SH, et al. (2010) A V3 loop-dependent gp120 element disrupted by CD4 binding stabilizes the human immunodeficiency virus envelope glycoprotein trimer. *J Virol* 84(7):3147–3161.
37. Walker LM, et al.; Protocol G Principal Investigators (2009) Broad and potent neutralizing antibodies from an African donor reveal a new HIV-1 vaccine target. *Science* 326(5950):285–289.
38. McLellan JS, et al. (2011) Structure of HIV-1 gp120 V1/V2 domain with broadly neutralizing antibody PG9. *Nature* 480(7377):336–343.
39. Dimitrov AS, Louis JM, Bewley CA, Clore GM, Blumenthal R (2005) Conformational changes in HIV-1 gp41 in the course of HIV-1 envelope glycoprotein-mediated fusion and inactivation. *Biochemistry* 44(37):12471–12479.
40. Mische CC, et al. (2005) An alternative conformation of the gp41 heptad repeat 1 region coiled coil exists in the human immunodeficiency virus (HIV-1) envelope glycoprotein precursor. *Virology* 338(1):133–143.
41. Sen J, et al. (2010) Alanine scanning mutagenesis of HIV-1 gp41 heptad repeat 1: Insight into the gp120-gp41 interaction. *Biochemistry* 49(24):5057–5065.
42. Yuan W, Bazick J, Sodroski J (2006) Characterization of the multiple conformational states of free monomeric and trimeric human immunodeficiency virus envelope glycoproteins after fixation by cross-linker. *J Virol* 80(14):6725–6737.
43. Wu X, et al. (2010) Rational design of envelope identifies broadly neutralizing human monoclonal antibodies to HIV-1. *Science* 329(5993):856–861.
44. Wu X, et al. (2009) Mechanism of human immunodeficiency virus type 1 resistance to monoclonal antibody B12 that effectively targets the site of CD4 attachment. *J Virol* 83(21):10892–10907.
45. Diskin R, et al. (2011) Increasing the potency and breadth of an HIV antibody by using structure-based rational design. *Science* 334(6060):1289–1293.
46. Pancera M, Wyatt R (2005) Selective recognition of oligomeric HIV-1 primary isolate envelope glycoproteins by potently neutralizing ligands requires efficient precursor cleavage. *Virology* 332(1):145–156.
47. Tran EEH, et al. (2012) Structural mechanism of trimeric HIV-1 envelope glycoprotein activation. *PLoS Pathog* 8(7):e1002797.
48. Haim H, Salas I, Sodroski J (2013) Proteolytic processing of the human immunodeficiency virus envelope glycoprotein precursor decreases conformational flexibility. *J Virol* 87(3):1884–1889.
49. Carr CM, Kim PS (1993) A spring-loaded mechanism for the conformational change of influenza hemagglutinin. *Cell* 73(4):823–832.
50. Wilson IA, Skehel JJ, Wiley DC (1981) Structure of the haemagglutinin membrane glycoprotein of influenza virus at 3 A resolution. *Nature* 289(5796):366–373.
51. Binley JM, et al. (2000) A recombinant human immunodeficiency virus type 1 envelope glycoprotein complex stabilized by an intermolecular disulfide bond between the gp120 and gp41 subunits is an antigenic mimic of the trimeric virion-associated structure. *J Virol* 74(2):627–643.
52. Yang X, Farzan M, Wyatt R, Sodroski J (2000) Characterization of stable, soluble trimers containing complete ectodomains of human immunodeficiency virus type 1 envelope glycoproteins. *J Virol* 74(12):5716–5725.

Supporting Information

Mao et al. 10.1073/pnas.1307382110

SI Materials and Methods

Protein Expression and Purification. Details of HIV-1 Env expression and purification have been described previously (1). In brief, *env* DNA encoding the HIV-1_{JR-FL} membrane-bound HIV-1 Env trimer [Env(-)ΔCT] glycoprotein was codon-optimized and subcloned into the pcDNA3.1(-) expression plasmid (Invitrogen). The Env(-)ΔCT glycoprotein was transiently expressed in 293F cells. Thirty-six hours after transfection, cells expressing the envelope glycoproteins were harvested by spinning the cell suspension at 100 × *g* for 5 min at 4 °C, followed by washing with PBS at 4 °C. The cell pellets were resuspended in approximately five volumes of homogenization buffer [250 mM sucrose, 10 mM Tris·HCl (pH 7.4), and a mixture of protease inhibitors (Roche Complete tablets)]. The resuspended cells were homogenized in a 50-mL glass Dounce homogenizer on ice. The homogenate was spun at 600 × *g* for 10 min at 4 °C. The pellet was discarded, and the supernatant was collected and spun at 8,000 × *g* for 10 min at 4 °C. The supernatant solution was collected and was ultracentrifuged at 100,000 × *g* for 30 min at 4 °C. The pellet containing plasma membranes was collected and the supernatant discarded. The pellet was resuspended in homogenization buffer and was homogenized in a 15-mL glass Dounce homogenizer and ultracentrifuged at 100,000 × *g* for 45 min at 4 °C. The pellet containing purified plasma membrane was collected and solubilized in a solubilization buffer containing 100 mM $(NH_4)_2SO_4$, 20 mM Tris·HCl (pH 8), 300 mM NaCl, 20 mM imidazole, 1% (wt/vol) Cymal-5 (Affymetrix), and a mixture of protease inhibitors (Roche Complete tablets). The membranes were solubilized by incubation at 4 °C for 30 min on a rocking platform. The suspension was ultracentrifuged for 30 min at 200,000 × *g* at 4 °C. The supernatant was collected and mixed with a small volume of preequilibrated Ni-NTA beads (Qiagen) for 8–12 h on a rocking platform at 4 C°. The mixture was then injected into a small column and washed with a buffer containing 100 mM $(NH_4)_2SO_4$, 20 mM Tris·HCl (pH 8), 1 M NaCl, 30 mM imidazole, 0.5% Cymal-5 (for 1-mL Ni-NTA beads, we used ∼15–30 mL buffer for washing). The well-washed bead-filled column was eluted with a buffer containing 100 mM $(NH_4)_2SO_4$, 20 mM Tris·HCl (pH 7.4), 250 mM NaCl, 250 mM imidazole, and 0.5% Cymal-5. The eluted Env(-)ΔCT glycoprotein solution was concentrated, diluted in a buffer containing 20 mM Tris·HCl (pH 7.4), 300 mM NaCl, and 0.01% Cymal-6, and reconcentrated to 1.5–2.5 mg/mL before cryo-sample preparation.

Cryo-EM Data Collection. To prepare the cryo-sample for single-particle imaging, 2.5 μL of the 1.5–2.5 mg mL^{-1} Env(-)ΔCT solution was spread on a C-flat holey carbon grid (Electron Microscopy Sciences) in a chamber of 100% humidity, held for 2 s, blotted with filter paper for 2 s at 4 °C, and then flash-plunged into liquid ethane by Vitrobot (FEI). The prepared cryo-grids were transferred into the CT3500 cryo-transfer system (Gatan) in liquid nitrogen and were used for single-particle image data collection at −183 °C. Focus pairs of micrographs were recorded on a Tecnai F20 TEM (FEI) with a field-emission gun at 200 kV and a calibrated magnification of 200,835× on a 4k × 4k Ultrascan CCD camera (Gatan). The electron dose of each exposure was 10–15 electrons $Å^{-2}$. The defocus of the second set of micrographs differed from that of the first set by 1.0 μm. The majority of accumulated image data were collected with the assistance of the Leginon automated imaging system (2) in a semiautomatic fashion.

Image Processing and 3D Reconstruction. Micrographs were screened for drift, astigmatism, and visibility of Thon rings in the power spectra. Parameters of the contrast transfer function (CTF) of each micrograph were determined with the CTFFind3 program (3, 4). A total of 670,000 single-particle images (with dimensions of 256 × 256 pixels and a pixel size of 0.747 Å) selected from the closer-to-focus micrographs were used for structure refinement. The defocus ranged from −350 to −3,000 nm. The quality and selection of these particle images were evaluated and verified comprehensively by unsupervised classification using multivariate data analysis and K-means clustering, as previously described (5). Each single-particle image was decimated by 4 times to a dimension of 64 × 64 pixels, and was low-pass filtered at 12 Å for particle verification. The initial alignment for projection Euler angles and in-plane shift was generated by the projection-matching algorithm using a previously determined 11-Å map of the same Env construct as an initial reference (Electron Microscopy Data Bank accession code: EMD-5418). The particles images were grouped into 57 defocus groups, with a defocus width of 20 nm in each group before refinement. The back-projection reconstruction at each iteration of the refinement was CTF-corrected by Wiener filtering (6, 7). The angular increment was progressively decreased from 10° to 0.5° in the refinement. The resolution of the reconstruction was measured by both conventional Fourier shell correlation (FSC) (8, 9) and the "gold-standard" FSC (10, 11). The latter was calculated by two half datasets that were refined fully independently from each other, keeping all but the initial reference separate (10). The former approach estimated a final resolution of 5.5 Å by conventional FSC at 0.5 cutoff, and the latter approach estimated a final resolution of 6 Å by the "gold-standard" FSC at 0.5 cutoff. The final map obtained by the "gold standard" refinement protocol was deconvoluted and amplitude-corrected by a B-factor of −150 $Å^2$ and was low-pass filtered at 5.8 Å with a cosine edge of 8-Fourier-pixel width (12, 13). The above image analysis was implemented in customized computational procedures and workflows, combining the functions of SPIDER (14) and XMIPP (15).

Structure Analysis. Segmentation of the cryo-EM density was done in University of California, San Francisco (UCSF) Chimera (16). Fitting of crystal structures and secondary structure elements in the cryo-EM map was performed in O (17) and Coot (18). The secondary structure elements of the glycoprotein (gp)120 inner domain were positioned by flexibly fitting the crystal structure of the CD4-bound gp120 core [Protein Data Bank (PDB) ID: 3JWD] to the cryo-EM map by the Flex-EM program (1), based on molecular dynamics simulations in Modeler (20) and by energetic optimization in CNS (21). Analysis of CD4BS antibody interaction with the Env trimer was done by fitting the gp120 outer domain from the antibody:gp120 core complex crystal structure to the cryo-EM map in a rigid-body fashion in Coot and UCSF Chimera. Graphics were done in PyMOL (Schrodinger) and UCSF Chimera.

Cell-Based ELISA. Ligand binding to trimeric envelope glycoproteins on the surface of COS-1 or HOS.pBABEpuro cells [ATCC and National Institutes of Health (NIH) AIDS Research and Reference Reagent Program, respectively] was measured by a cell-based ELISA, as previously described (22). In brief, COS-1 or HOS cells were seeded in 96-well plates (2×10^4 cells per well) and transfected the next day with 0.15 μg per well of plasmid DNA expressing the codon-optimized (GenScript) genes encoding the HIV-1_{JR-FL} wild-type Env, Env(+)ΔCT (cleavage-competent,

cytoplasmic tail-deleted) and Env(-)ΔCT (cleavage-negative, cytoplasmic tail-deleted) glycoproteins using the standard polyethylenimine (PEI; Polyscience) transfection method. The Env proteolytic cleavage site was altered by R508S and R511S changes; the Env cytoplasmic tail was truncated by substitution of a stop codon for codon 712. Two days after the transfection, the cells were washed twice with blocking buffer [10 mg/mL nonfat dry milk, 1.8 mM $CaCl_2$, 1 mM $MgCl_2$, 25 mM Tris (pH 7.5), and 140 mM NaCl] and then incubated for 1 h at room temperature with Env ligands. The ligands tested were polyclonal antibodies in a pool of heat-inactivated sera from HIV-1–infected individuals (used at 1/2,000 dilution); a 1-μg/mL dilution of CD4-Ig [a fusion protein in which the N-terminal two domains of CD4 are linked to the Fc component of IgG (23)]; or anti-HIV-1 Env monoclonal antibodies VRC01, b12, b13, F105, 17b, 2G12, 2F5, 4e10, A32, C11, PGT121, and PGT126 at a 1-μg/mL dilution. An HRP-conjugated antibody specific for the Fc region of human IgG (Pierce) was then incubated with the samples for 45 min at room temperature. Cells were washed five times with blocking buffer and five times with washing buffer. HRP enzyme activity was determined after the addition of 30 μL per well of a 1:1 mix of Western Lightning oxidizing and luminol reagents (Perkin-Elmer Life Sciences). Light emission was measured with an LB 941 TriStar luminometer (Berthold Technologies). The following reagents were obtained through the NIH AIDS Research and Reference Reagent Program, Division of AIDS, National Institute of Allergy and Infectious Diseases, NIH: monoclonal antibodies to HIV-1 gp41 (98-6, 126-7, 246-D, 240-D, 50-69) from S. Zolla-Pazner; HIV-1 gp41 monoclonal antibodies (4E10, 5F3) from H. Katinger; and HIV-1 gp41 monoclonal antibody (F240) from M. Posner and L. Cavacini.

1. Mao Y, et al. (2012) Subunit organization of the membrane-bound HIV-1 envelope glycoprotein trimer. *Nat Struct Mol Biol* 19(9):893–899.
2. Suloway C, et al. (2005) Automated molecular microscopy: The new Leginon system. *J Struct Biol* 151(1):41–60.
3. Huang Z, Baldwin PR, Mullapudi S, Penczek PA (2003) Automated determination of parameters describing power spectra of micrograph images in electron microscopy. *J Struct Biol* 144(1-2):79–94.
4. Mindell JA, Grigorieff N (2003) Accurate determination of local defocus and specimen tilt in electron microscopy. *J Struct Biol* 142(3):334–347.
5. Shaikh TR, Trujillo R, LeBarron JS, Baxter WT, Frank J (2008) Particle-verification for single-particle, reference-based reconstruction using multivariate data analysis and classification. *J Struct Biol* 164(1):41–48.
6. Frank J (2006) *Three-Dimensional Electron Microscopy of Macromolecular Assemblies: Visualization of Biological Molecules in Their Native State* (Oxford Univ Press, Oxford).
7. Penczek PA (2010) Image restoration in cryo-electron microscopy. *Methods Enzymol* 482:35–72.
8. Penczek PA (2010) Resolution measures in molecular electron microscopy. *Methods Enzymol* 482:73–100.
9. Liao HY, Frank J (2010) Definition and estimation of resolution in single-particle reconstructions. *Structure* 18(7):768–775.
10. Grigorieff N (2000) Resolution measurement in structures derived from single particles. *Acta Crystallogr D Biol Crystallogr* 56(Pt 10):1270–1277.
11. Scheres SHW, Chen S (2012) Prevention of overfitting in cryo-EM structure determination. *Nat Methods* 9(9):853–854.
12. Rosenthal PB, Henderson R (2003) Optimal determination of particle orientation, absolute hand, and contrast loss in single-particle electron cryomicroscopy. *J Mol Biol* 333(4):721–745.
13. Fernández JJ, Luque D, Castón JR, Carrascosa JL (2008) Sharpening high resolution information in single particle electron cryomicroscopy. *J Struct Biol* 164(1):170–175.
14. Shaikh TR, et al. (2008) SPIDER image processing for single-particle reconstruction of biological macromolecules from electron micrographs. *Nat Protoc* 3(12):1941–1974.
15. Scheres SHW, Núñez-Ramírez R, Sorzano COS, Carazo JM, Marabini R (2008) Image processing for electron microscopy single-particle analysis using XMIPP. *Nat Protoc* 3(6):977–990.
16. Pettersen EF, et al. (2004) UCSF Chimera—a visualization system for exploratory research and analysis. *J Comput Chem* 25(13):1605–1612.
17. Jones TA (2004) Interactive electron-density map interpretation: From INTER to O. *Acta Crystallogr D Biol Crystallogr* 60(Pt 12 Pt 1):2115–2125.
18. Emsley P, Lohkamp B, Scott WG, Cowtan K (2010) Features and development of Coot. *Acta Crystallogr D Biol Crystallogr* 66(Pt 4):486–501.
19. Topf M, et al. (2008) Protein structure fitting and refinement guided by cryo-EM density. *Structure* 16(2):295–307.
20. Martí-Renom MA, et al. (2000) Comparative protein structure modeling of genes and genomes. *Annu Rev Biophys Biomol Struct* 29:291–325.
21. Brunger AT (2007) Version 1.2 of the Crystallography and NMR system. *Nat Protoc* 2(11):2728–2733.
22. Haim H, et al. (2009) Soluble CD4 and CD4-mimetic compounds inhibit HIV-1 infection by induction of a short-lived activated state. *PLoS Pathog* 5(4):e1000360.
23. Herschhorn A, Marasco WA, Hizi A (2010) Antibodies and lentiviruses that specifically recognize a T cell epitope derived from HIV-1 Nef protein and presented by HLA-C. *J Immunol* 185(12):7623–7632.

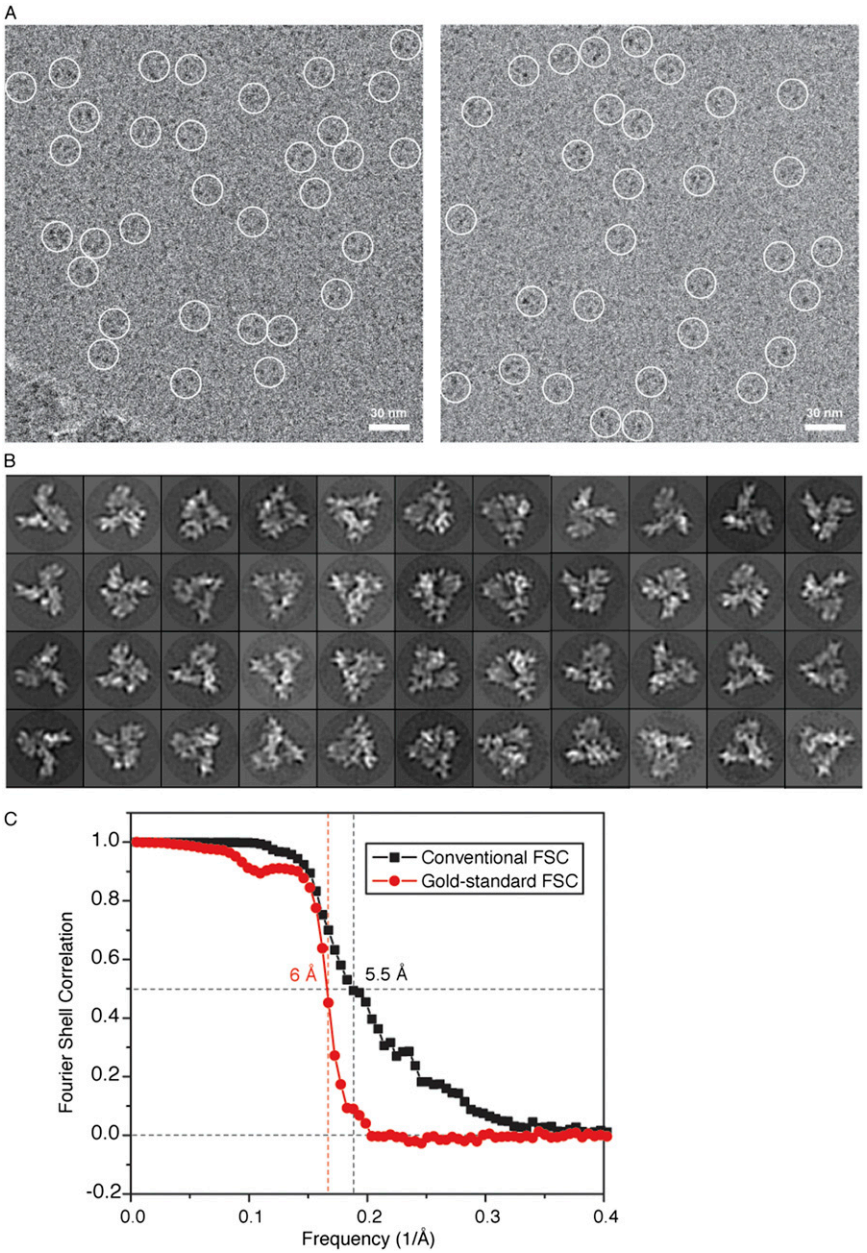

Fig. S1. Cryo-EM imaging and resolution assessment. (*A*) Two typical 4k × 4k micrographs of the purified HIV-1_{JR-FL}Env(-)ΔCT trimers protected by the Cymal-6 detergent and embedded in a vitreous ice film. The micrograph shown is low-pass filtered at 1.0 nm. A number of candidate single-particle projections of the Env trimer are highlighted by white circles. Defocus of the micrograph is ~3 μm. (*B*) Gallery of selected typical class-average images after initial alignment and 2D refinement. Note the improved structural details not evident in the raw images and not apparent in the previously reported lower-resolution model (1). (*C*) Resolution measurement of the cryo-EM structure of the HIV-1_{JR-FL}Env(-)ΔCT trimer, using both the conventional FSC approach at FSC-0.5 cutoff and the gold standard FSC approach at 0.5 cutoff. The conventional FSC (black curve) was calculated between two separate reconstructions, each generated from a randomly divided half of the entire dataset, both of which were refined with a single common reference. The gold standard FSC (red curve) was calculated between two half-set reconstructions that were refined independently with two fully separate references. The conventional FSC at 0.5 cutoff yielded a slightly higher estimate of resolution compared with the gold standard FSC at 0.5 cutoff. The reported resolution is based on the gold standard FSC approach.

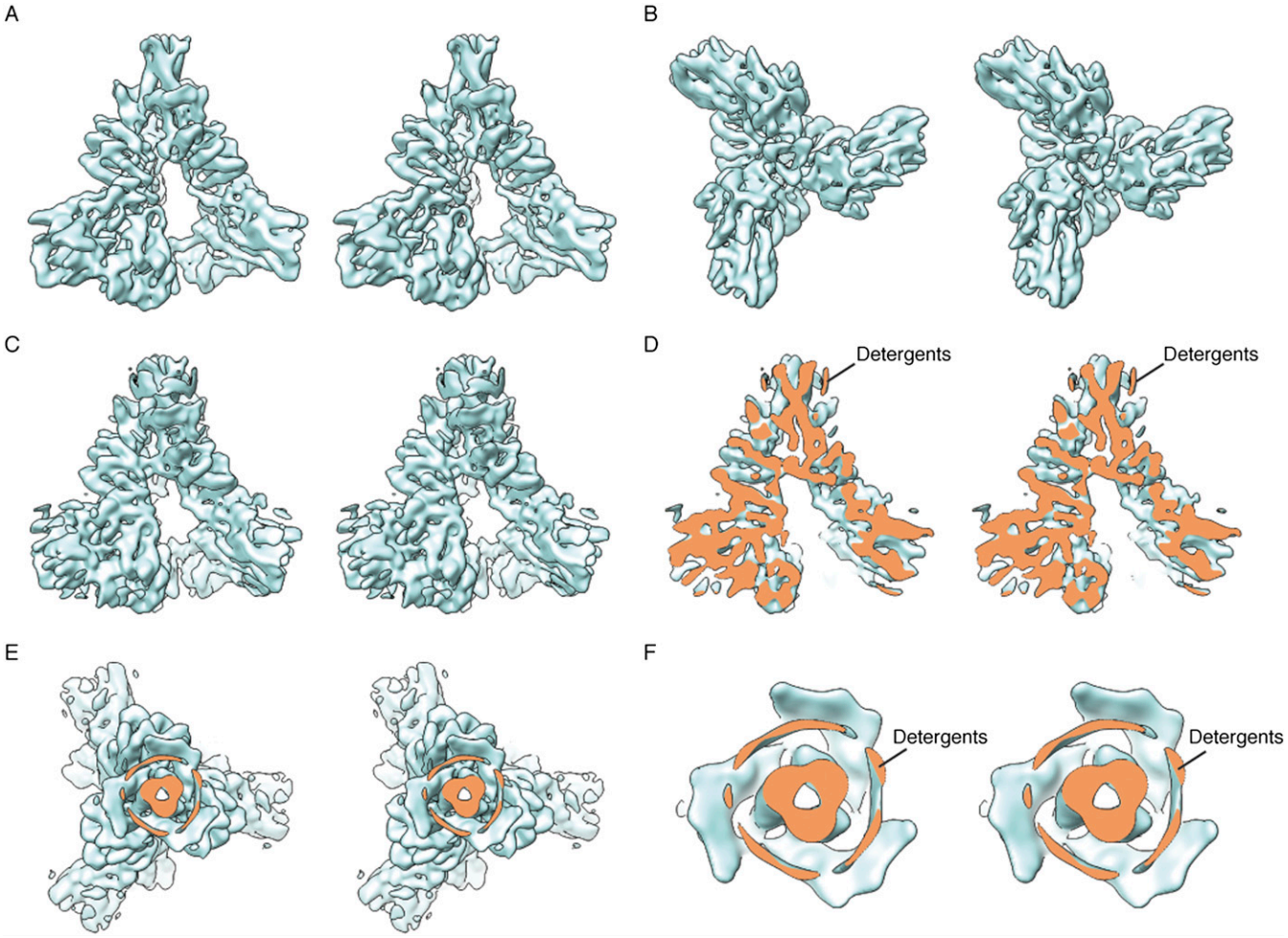

Fig. S2. Stereo views of the overall cryo-EM structure of the HIV-1_{JR-FL}Env trimer. (*A*) Stereo view of the cryo-EM map in an isosurface representation, viewed from a perspective parallel to the viral membrane. (*B*) Stereo view of the same isosurface, viewed from the perspective of the target cell. (*C*) Stereo view of the cryo-EM map in an isosurface representation at a lower level of contour compared with that in *A* and *B*, viewed from a perspective parallel to the viral membrane. (*D*) Stereo view of the same isosurface as that shown in *C*, with its central cross-section clipped. (*E*) Stereo view of the cryo-EM map in the same isosurface representation as that shown in *C*, viewed from a perspective from the interior of the virus, with the cross-section of the transmembrane region clipped. (*F*) Stereo view of a close-up of the cross-section of the transmembrane region, showing three separated thin layers, which likely represent detergent molecules surrounding the transmembrane helices.

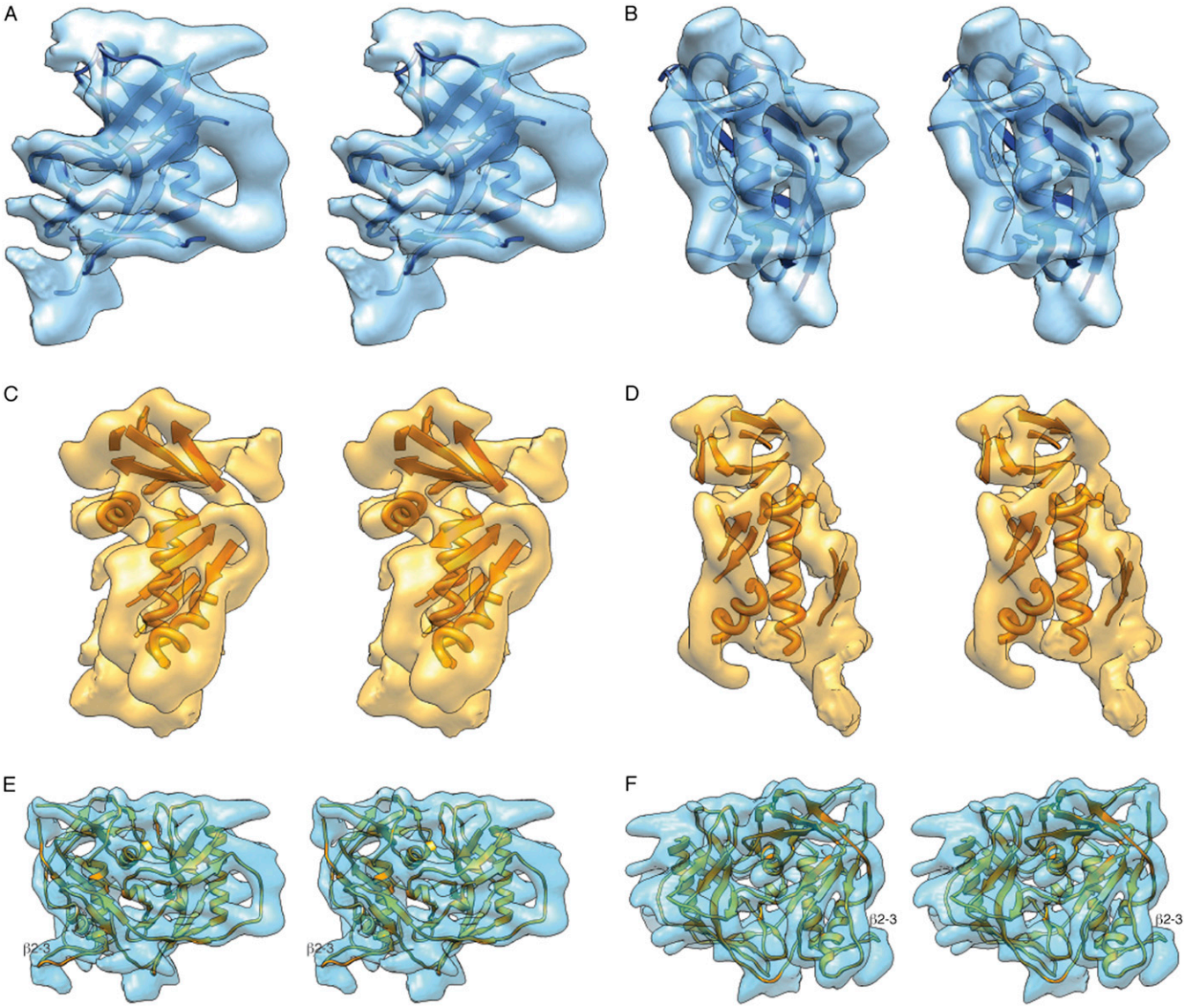

Fig. S3. Stereo views of the unliganded gp120 core structure fitted in the cryo-EM map. (*A*) Cryo-EM density segment associated with the gp120 outer domain is shown as a transparent isosurface. The crystal structure of the outer domain of the gp120 core is fitted into the cryo-EM density as a rigid body and is shown in ribbon representation. (*B*) Same isosurface as shown in *A*, rotated 90° around the vertical axis. The density associated with the gp120 V4 variable loop, which was not resolved in the crystal structure, is evident on the right-hand side of the molecule in *A* and projects toward the viewer in *B*. (*C*) The cryo-EM density segment associated with the gp120 inner domain is shown as a transparent isosurface. The secondary structure of the gp120 inner domain was assessed by flexible fitting, and the approximate positions of secondary structure elements are shown in cartoon representation. (*D*) Stereo view of the same density as in *C*, rotated 90° around the vertical axis. (*E* and *F*) Crystal structure of the gp120 core was flexibly fitted into the cryo-EM density segment associated with the overall gp120 core, from two opposite perspectives.

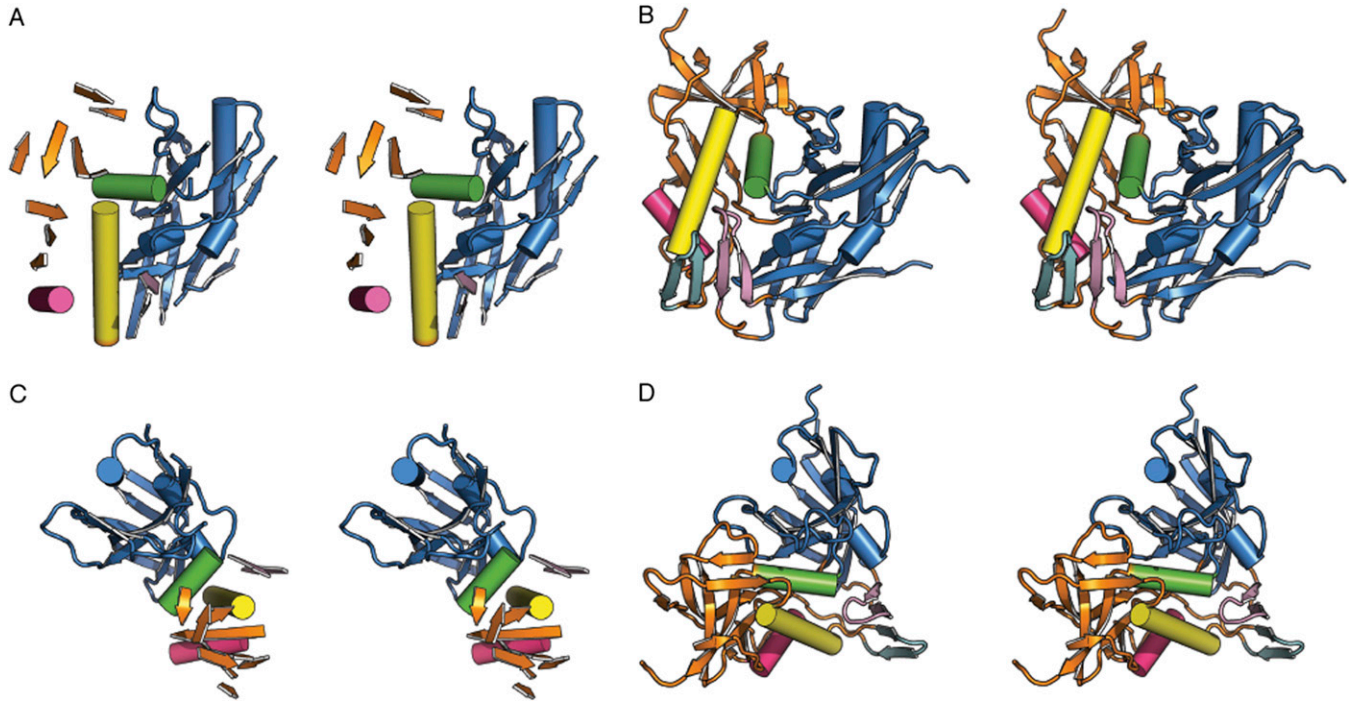

Fig. S4. Stereo views of the comparison between the conformations of the unliganded gp120 core in the Env trimer and the monomeric CD4-bound gp120 core. (*A* and *C*) Stereo views of the secondary structures in the gp120 core that was flexibly fitted to the unliganded state of the Env trimer. (*B* and *D*) Stereo views of a ribbon representation of the CD4-bound monomeric gp120 core (PDB ID: 3JWD). For comparison between the unliganded state and the CD4-bound state, the gp120 outer domains (blue) are aligned in the same orientation between *A* and *B*, and between *C* and *D*. The view in *A* and *B* is from a perspective roughly parallel to the viral membrane. The view in *C* and *D* is from the perspective of the viral membrane.

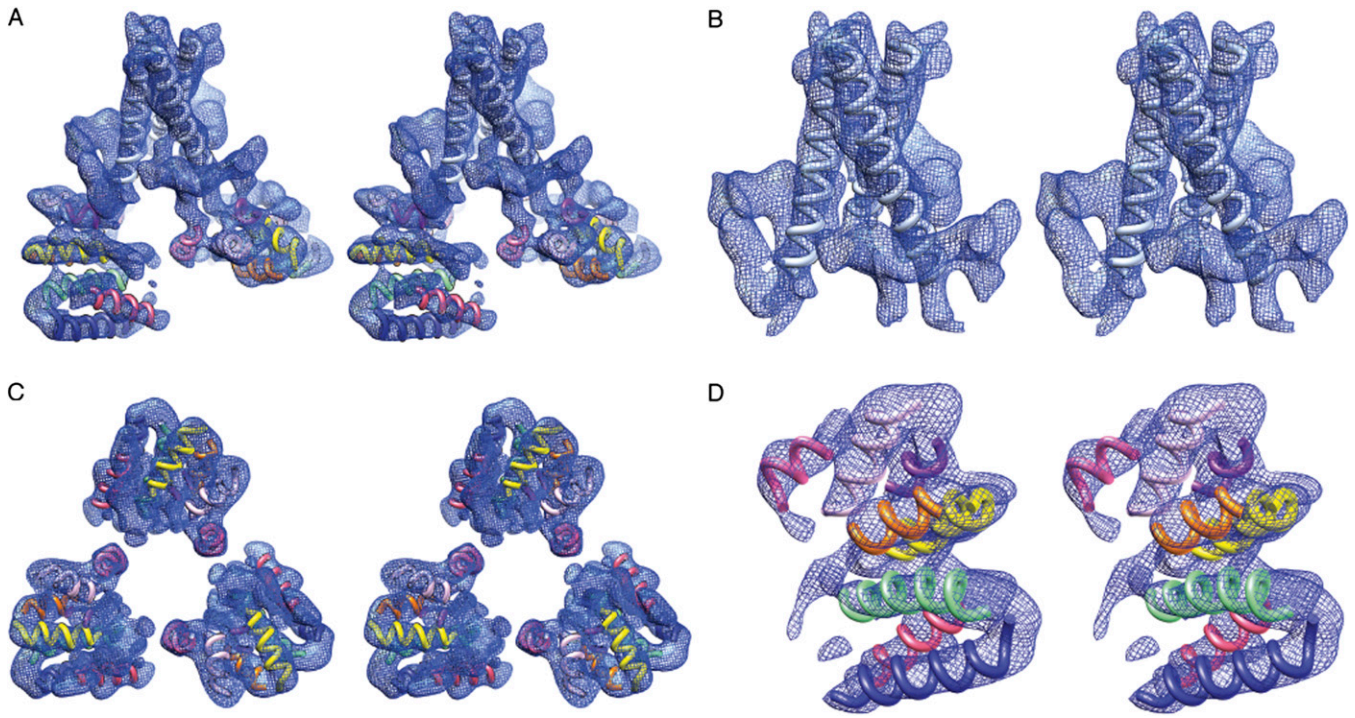

Fig. S5. Stereo views of the gp41 structure. (*A*) Stereo view of the density associated with the three gp41 subunits in the Env trimer, viewed from an angle of 30° with respect to the viral membrane. (*B*) Stereo view of the segmented density of the gp41 membrane-interactive region, viewed from the same perspective as that in *A*. (C) Stereo view of the density associated with the gp41 ectodomain, viewed from the perspective of the viral membrane. (*D*) Stereo view of the gp41 ectodomain, from a perspective parallel to the viral membrane.

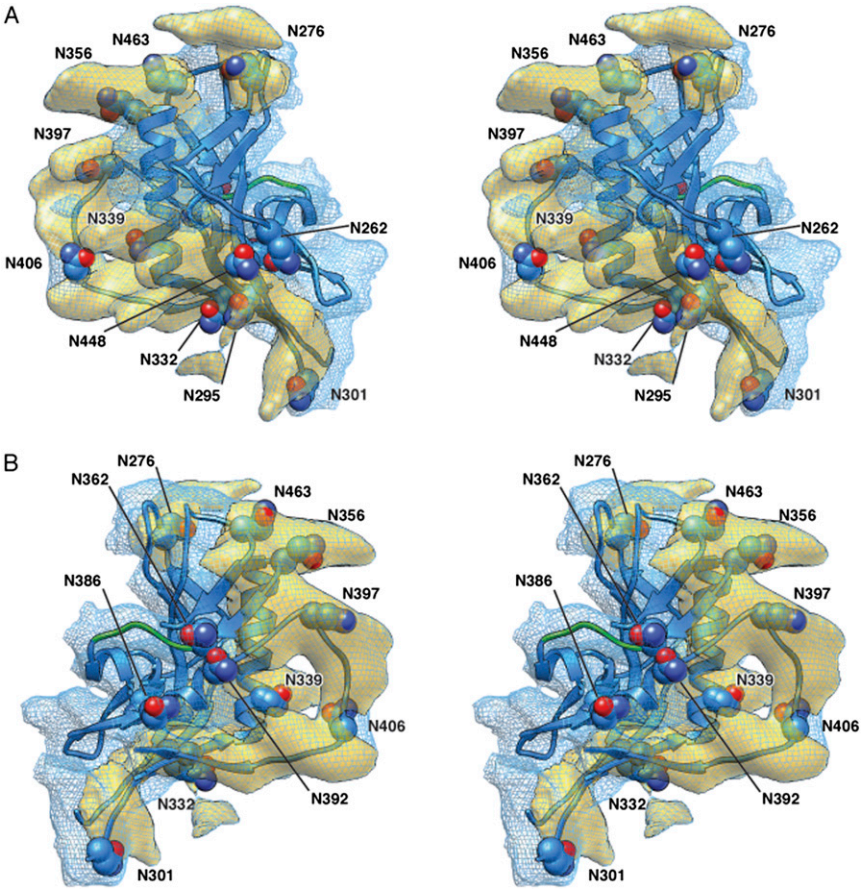

Fig. S6. Stereo views of gp120 glycan-associated density. (*A*) Stereoview of the glycan-associated densities on the gp120 surface, viewed from a perspective parallel to the viral membrane. The gp120 outer domain ribbon is colored blue, and the asparagine residues associated with potential *N*-linked glycosylation sites are depicted in Corey-Pauling-Koltun (CPK) representation and labeled. (*B*) Stereo view of the glycan-associated densities on the gp120 surface. The perspective is ~180° from that of *A*. These images reproduce Fig. 5 in stereo. The yellow densities highlight the glycan-associated cryo-EM segments.

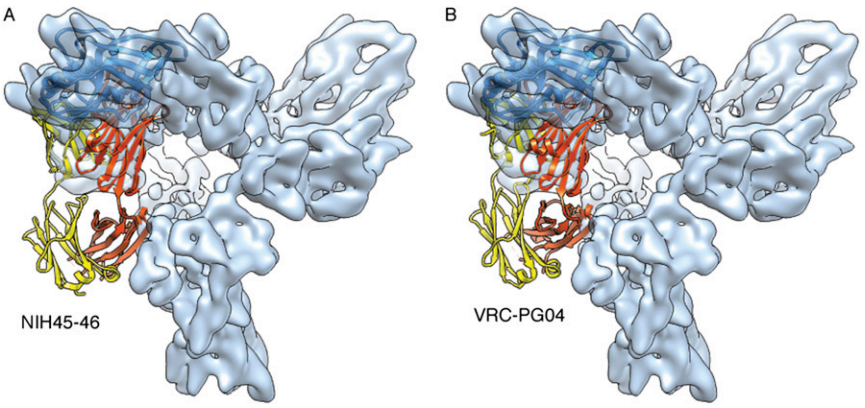

Fig. S7. Additional CD4BS antibody interactions with the Env trimer. Crystal structures of the gp120 core in complex with the CD4BS antibodies, NIH45-46 (*A*) and VRC-PG04 (*B*), were superposed on the unliganded Env trimer map as follows: the conformationally rigid gp120 outer domain was fitted to the Env trimer density map, and the outer domains in the crystal structures were aligned with the fitted outer domain (represented as a blue ribbon). These figures are an extension of Fig. 6, with the complexes viewed from the perspective shown in that figure. The PDB IDs of the antibodies in complex with gp120 core structures are 3U7Y (*A*) and 3SE9 (*B*).

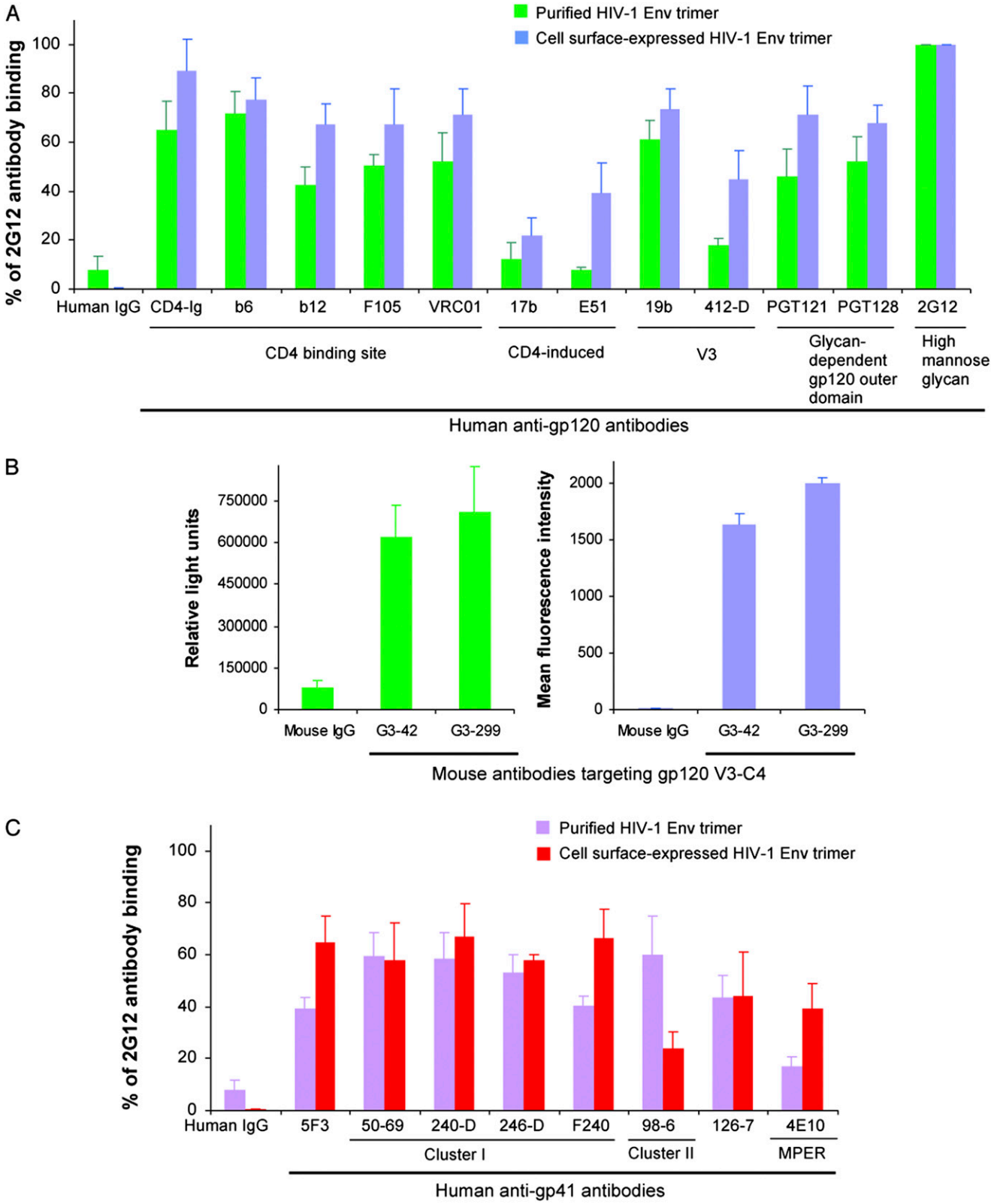

Fig. S8. Antigenic profile of the purified HIV-1 envelope trimer. The structural integrity of the purified HIV-1_{JR-FL}Env(-)ΔCT trimer was evaluated by testing the binding at 20 °C of a large panel of monoclonal antibodies and CD4-Ig to the purified trimer in an ELISA. Binding of the same ligands to an identical HIV-1_{JR-FL}Env(-)ΔCT trimer expressed transiently on the surface of transfected cells was measured at 20 °C by flow cytometry and served as a reference. Under the conditions of these experiments [and in contrast to the modeling of the fixed Env(-)ΔCT trimer in Fig. 6], the Env(-)ΔCT glycoprotein can undergo conformational changes during incubation with the antibody. (*A*) Binding of conformation-dependent antibodies to the indicated epitopes on HIV-1 gp120. (*B*) Binding of mouse antibodies directed against conformation-dependent epitopes comprising the V3 region and the fourth conserved region (C4) of HIV-1 gp120. Antibody binding to detergent-solubilized, purified Env(-)ΔCT glycoprotein (green) and Env(-)ΔCT glycoprotein expressed on cell surfaces (blue) is

Legend continued on following page

shown. (C) Binding of antibodies to different regions on HIV-1 gp41. Each ligand was tested at a single concentration of 10 μg/mL, and polyclonal human IgG (or mouse IgG) served as a negative control. The mean fluorescence intensity associated with the binding of the polyclonal human and mouse IgG negative controls to the cell surface-expressed Env was too low to be seen on the bar graph. Results shown represent the average of three independent experiments. V3, the third variable loop of gp120; C4, the fourth conserved region of gp120; cluster I, gp41 amino acids 597–613; cluster II, gp41 amino acids 644–663; MPER, membrane-proximal external region.

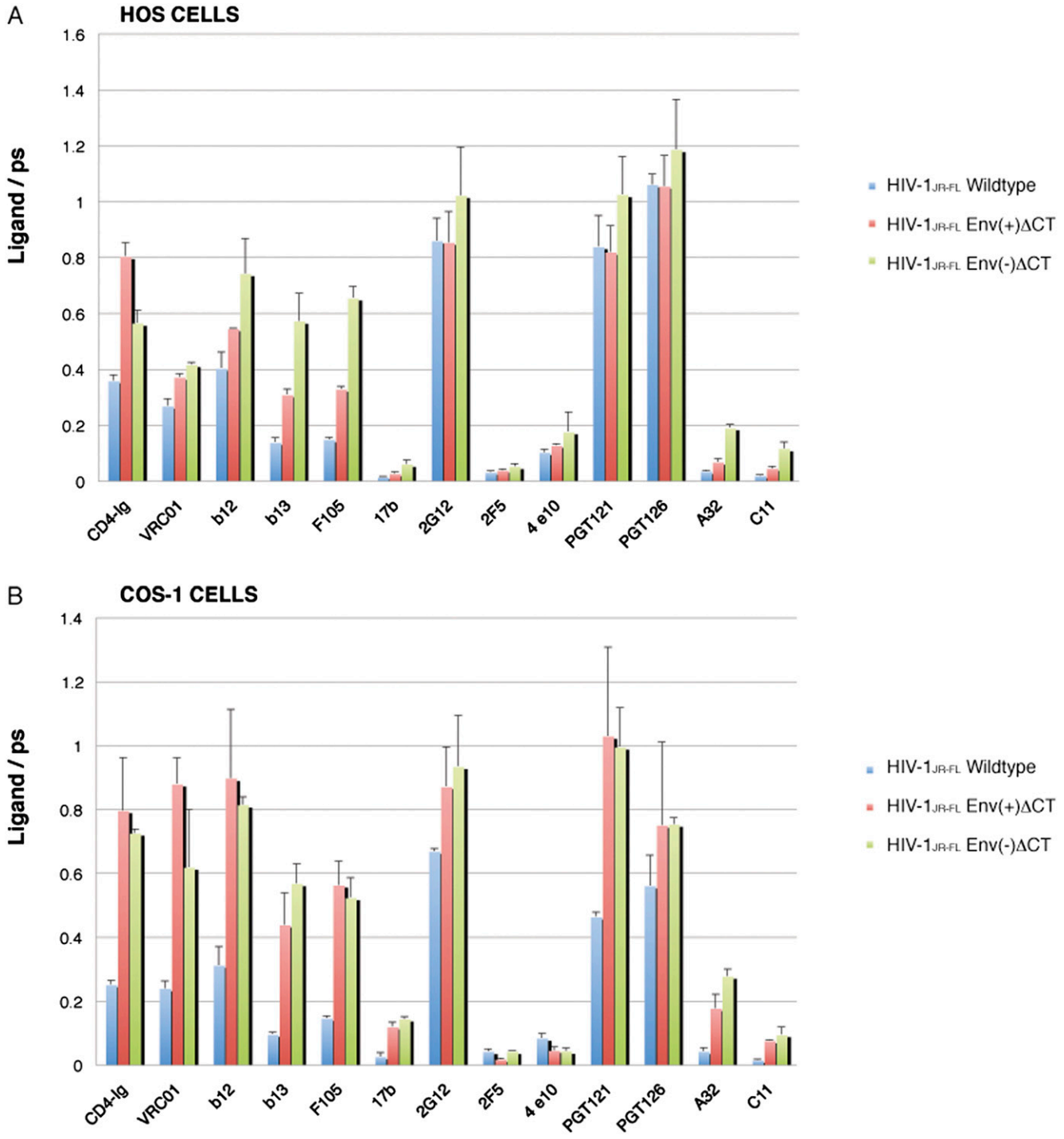

Fig. S9. Binding of cell-surface HIV-1_{JR-FL}Env variants by Env ligands. The binding of Env ligands (CD4-Ig and monoclonal antibodies) was measured to three HIV-1_{JR-FL}Env variants: wild-type Env; Env(+)ΔCT (intact proteolytic cleavage site, truncated cytoplasmic tail), and Env(-)ΔCT (modified proteolytic cleavage site, truncated cytoplasmic tail), using a cell-based ELISA. The Env variants were expressed in transfected HOS (*A*) or COS-1 (*B*) cells. Proteolytic cleavage of the wild-type Env and Env(+)ΔCT glycoproteins was more efficient in HOS cells than in COS-1 cells. The Env ligands were CD4-Ig, CD4-binding site antibodies (VRC01, b12, b13, F105), a CD4-induced antibody (17b), glycan-dependent antibodies (2G12, PGT121, PGT126), an inner domain-specific antibody (A32), an antibody against the gp120 N/C termini (C11), and antibodies against the gp41 MPER (2F5, 4E10). Results were normalized to the signal obtained with pooled sera (ps) from HIV-1–infected individuals. Results are representative of at least two independent experiments, each performed in duplicate.

Table S1. Quantitative evaluation of the goodness of fit

Parameter	No. of residues in the density	No. of residues out of the density	No. of total residues fitted	Goodness of fit (%)
Rigid-body fit of gp120 outer domain	127	14	141	90
Flexible fit of gp120 outer domain	150	1	151	99.3
Flexible fit of gp120 inner domain	190	4	194	98
Flexible fit of gp120 core	340	5	345	98.6
Gp120 TAD helix	12	0	12	100
Gp41 helix 1	28	0	28	100
Gp41 helix 2	5	0	5	100
Gp41 helix 3	10	0	10	100
Gp41 helix 4	5	0	5	100
Gp41 helix 5	10	0	10	100
Gp41 helix 6	16	1	17	94
Gp41 helix 7	16	0	16	100
Gp41 helix 8	17	0	17	100
Gp41 helix 9	15	0	15	100

The contour level of the density used to assess the fit is 2σ. The goodness of fit is indicated as the percent of the backbone residues inside the density. The side-chain fit was not taken into account in the evaluation. The numbering of gp41 helices is roughly proportional to their distance from the C terminus of the transmembrane region.

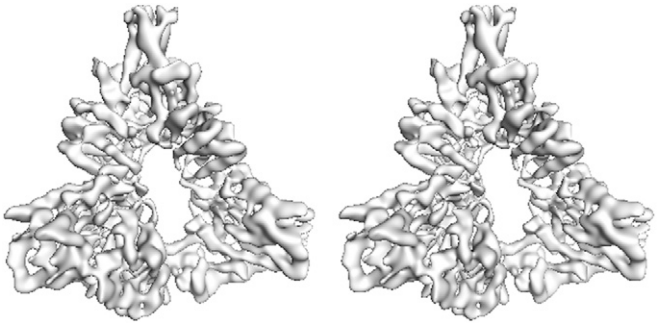

Movie S1. Side-by-side 3D movie showing the cryo-EM map of the unliganded HIV-1 envelope glycoprotein trimer. The cryo-EM density is shown at 3σ level.

Movie S1

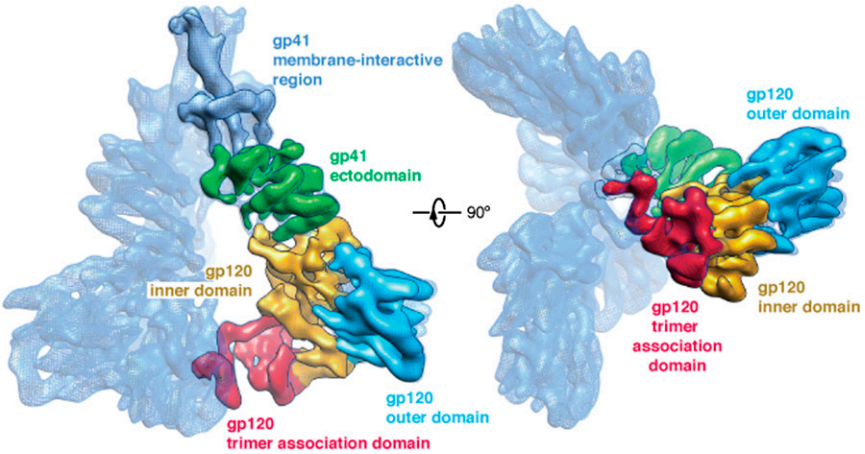

Movie S2. Side-by-side 3D movie showing the domain-based map segmentation of the cryo-EM structure of the unliganded HIV-1 envelope glycoprotein trimer.

Movie S2